

M.V. BONDAR,¹ O.V. PRZHONSKA,¹ O.D. KACHKOVSKY,² A. FRAZER,³
A.R. MORALES,³ K.D. BELFIELD³

¹Institute of Physics

(46, Prosp. Nauky, Kyiv 03028, Ukraine)

²Institute of Organic Chemistry

(5, Murmanskaya Str., Kyiv 03094, Ukraine)

³Department of Chemistry, University of Central Florida

(P.O. Box 162366, Orlando, FL 32816-2366, USA)

NEW FLUORENE-BASED FLUORESCENT PROBE WITH EFFICIENT TWO-PHOTON ABSORPTION

PACS 33.20.-t, 33.50.Dg

The synthesis, linear photophysical characterization, and two-photon absorption (2PA) properties of new fluorene derivative 3,3'-(pyridine-2,6-diyl)bis(1-(7-(diphenylamino)-9,9-dihexyl-9H-fluoren-2-yl)propane-1,3-dione) (1) have been presented. The steady-state absorption, fluorescence and excitation anisotropy spectra along with the fluorescence decay kinetics of 1 are obtained in the solvents of different polarities at room temperature with respect to its potential application in bioimaging. The analysis of linear photophysical properties revealed a complicated nature of the main one-photon absorption band of 1, and the strong solvatochromic effect in steady-state fluorescence spectra is observed. The degenerate 2PA spectrum of 1 is measured in the spectral range 570–970 nm with the use of the open aperture Z-scan method under the 1-kHz femtosecond excitation, and the maximum values of two-photon action cross sections $\sim(100-130)$ GM are obtained. The nature of the linear absorption and the 2PA bands is analyzed by quantum chemical methods using a Gaussian program package.

Keywords: two-photon absorption, fluorene, Z-scan method.

1. Introduction

The synthesis and the photophysical characterization of new organic compounds with large two-photon absorption (2PA) cross sections are essential steps for the development of practically vital nonlinear optical materials [1–5]. Fluorene-based derivatives with extended π -conjugation are the promising candidates for many important applications such as high-density optical data storage [6, 7], 3D microfabrication [8], optical power limiting [9], upconverted lasing [10], two-photon photodynamic therapy [11, 12], and two-photon fluorescence bioimaging microscopy [13–15]. Multiphoton fluorescence microscopy is a powerful tool for the creation of high-quality biological images and for the study of a broad variety of dynamic processes in living cells [16–18]. This application is based on the development of highly fluorescent and photochemically stable molecules with large 2PA cross section, δ_{2PA} [13, 19]. Unfortunately,

most of the known fluorescent organic labels, which can be utilized in one-photon fluorescence bioimaging, are not optimized for two-photon excitation due to the relatively small 2PA cross sections $\delta_{2PA} \sim 10-100$ GM [20, 21] and corresponding action cross sections $\delta_{2PA}^{act} = \delta_{2PA} \Phi$ [22] (Φ is the value of fluorescence quantum yield). Fluorene derivatives, exhibiting the high fluorescence quantum yield and the high photochemical stability [23–25], can be successfully utilized as two-photon fluorescent labels [26–28]. It should be mentioned that the main principles of the design and the synthesis of fluorene-based compounds with large values of δ_{2PA} are sufficiently well established and described previously [29, 30]. According to these principles, the molecular structure should be consisted of the electron-donating or electron-withdrawing parts arranged in symmetric or nonsymmetric manner with a large amount of π -electrons [31, 32]. In the case where the molecular structure includes two or more chromophore systems, an additional specific effect on the 2PA efficiency within the main absorption band can be expected due to the intramolecular interaction between these chromophores [33, 34].

© M.V. BONDAR, O.V. PRZHONSKA,
O.D. KACHKOVSKY, A. FRAZER, A.R. MORALES,
K.D. BELFIELD, 2013

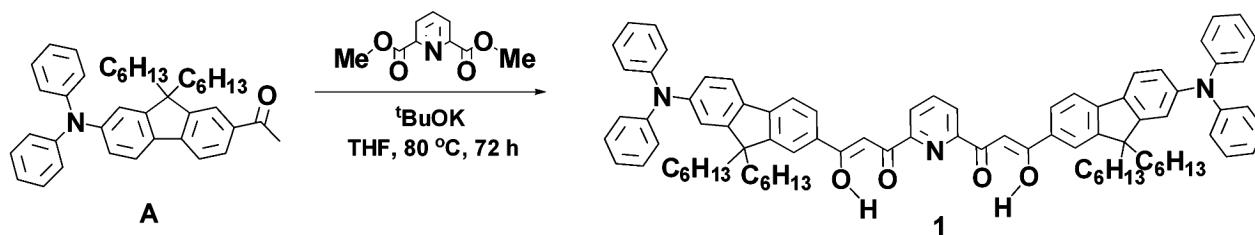


Fig. 1. Schematic of synthesis of **1**

In this paper, the linear photophysical and 2PA properties of the new fluorene derivative 3,3'-(pyridine-2,6-diyl)bis(1-(7-(diphenylamino)-9,9-dihexyl-9H-fluoren-2-yl)propane-1,3-dione) (**1**) as a promising candidate for two-photon fluorescence microscopy applications are investigated. A comprehensive analysis of the linear absorption and the fluorescence spectra of **1** is performed along with the steady-state excitation anisotropy and emission lifetime measurements. The values of 2PA cross sections, δ_{2PA} , were determined in a broad spectral range by the open aperture Z-scan method [35], by using the 1-kHz femtosecond excitation. The nature of the electronic structure of **1** and peculiarities of its linear and 2PA spectra are analyzed by quantum chemical calculations with the DFT and ZINDO-based methods implemented in the Gaussian 09 program package [36].

2. Experimental Section

2.1. Materials and synthetic procedures

The 1,5-pyridine-linked, bis-β-diketone compound **1** was synthesized through the Claisen condensation reaction of 1-(7-(diphenylamino)-9,9-dihexyl-9H-fluoren-2-yl)ethanone with dimethyl pyridine-2,6-dicarboxylate, using tertiary butoxide as a base. The schematic of the synthesis is shown in Fig. 1. 1-(7-bromo-9,9-dihexyl-9H-fluoren-2-yl)ethanone, being the precursor to the diphenylaminoketone 1-(7-(diphenylamino)-9,9-dihexyl-9H-fluoren-2-yl)ethanone (**A**), was prepared according to a literature procedure [37]. For the preparation of **1**, potassium tert-butoxide (0.62 g, 5.52 mmol) was added to a solution of dimethyl pyridine-2,6-dicarboxylate (0.17 g, 0.87 mmol) in THF (10 mL). The mixture underwent an immediate yellow color change. This was followed by the dropwise addition of a solution of 1-(7-(diphenylamino)-9,9-dihexyl-9H-fluoren-2-yl)ethanone (1.50 g, 2.76 mmol) in THF (15 mL)

over a period of 10 min. The resulting dark reaction mixture was then refluxed for 48 h stopped and then cooled to ambient. Hydrochloric acid (2M) was then added dropwise until a pH of 5 was obtained. Water (30 mL) was then added to the reaction mixture, and the organic phase extracted with dichloromethane. The combined extracts were then dried over anhydrous sodium sulfate. Volatiles were then removed to reveal brown oil. Purification was achieved using a silica column with a mobile phase of Hexane: Ethyl acetate 9.5: 0.5. Solvent was removed to reveal a yellow solid. Yield 0.60 g, 57%, mp 74–75 °C. ¹H NMR (500 MHz, CDCl₃) (ppm) 16.82 br, 2H enolic O–H, 8.32 d, 2H pyridine, 8.06 d 4H, 8.04, t 1H pyridine H₍₄₎, 7.76 m 4H, 7.59 d 2H, 7.25 m 6H, 7.14 10H, 7.02 m 8H, 3.73 q 2H, 2.01–1.89 m 8H, 1.25 s H₂O, 1.11–1.04 m 24H, 0.76 t 12H, 0.61 m 8H. ¹³C NMR (125 MHz, CDCl₃) (ppm) 187.22, 181.87, 153.40, 152.35, 151.16, 148.61, 147.70, 146.11, 138.25, 134.41, 133.04, 129.27, 127.02, 124.64, 124.33, 124.24, 123.05, 122.91, 121.62, 121.37, 118.97, 118.35, 93.60, 55.34, 40.25, 31.51, 29.57, 23.78, 22.53, 14.02. HRMS-ESI theoretical m/z [M+H]⁺ = 1217.7, found 1217.7, theoretical m/z [M+Na]⁺ = 1240.7, found 1240.7.

Structure determination of **1** was based on ¹H NMR, ¹³C NMR, and confirmed using high-resolution mass spectrometry. The ¹H NMR spectrum of this bis-β-diketone shows that its cis-enol isomer is the most dominant form, as evidenced by the presence of a broad resonance at $\sim\delta$ 16.82 ppm (enol protons) in CDCl₃, integrating to two protons. There was no evidence of a trans-enol tautomer, which proves the stability of the cis-form which allows for the 6-membered H-bonded ring in which the enolic H-atom can be envisaged as ligated by 2 oxygens.

2.2. Linear photophysical measurements

Linear photophysical properties of **1** were investigated in spectroscopic grade hexane (HEX), toluene

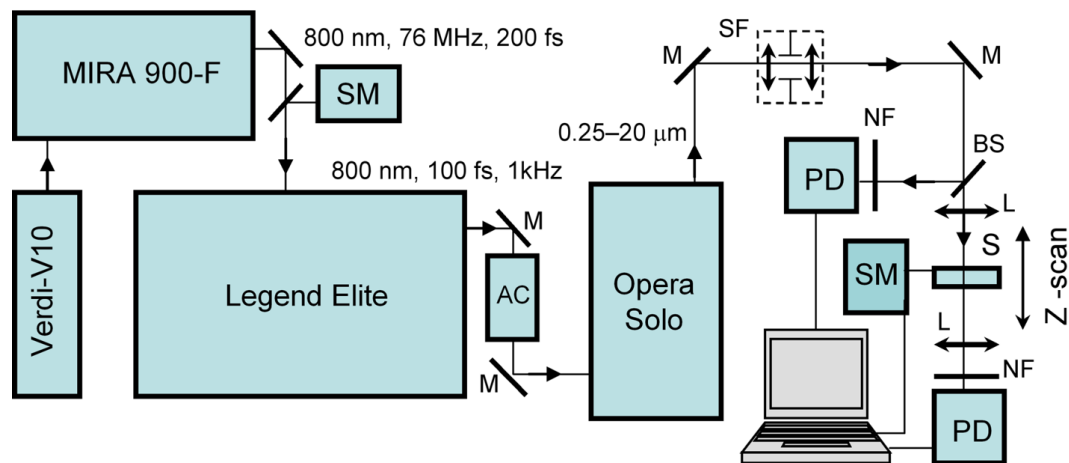


Fig. 2. Experimental setup (see the text for details): SM – laser spectrometer; AC – single-shot autocorrelator (Coherent Inc.); SF – space filter; M – 100% reflection Ag mirrors; L – focusing lenses; BS – beam splitter; NF – neutral density filters; PD – Si photodetectors; SM – step motor; S – sample

(TOL), tetrahydrofuran (THF) and dichloromethane (DCM) at room temperature. One-photon absorption (1PA) spectra of **1** were measured with an Agilent 8453 UV–visible spectrophotometer using 1 cm path length quartz cuvettes with molecular concentrations $C \sim 10^{-5}$ M. The steady-state fluorescence, excitation and excitation anisotropy spectra of **1** were obtained with a standard spectrofluorimeter (QuantaMaster, PTI Inc.) operating in the photon counting mode. All emission measurements were performed for low concentrated solutions, $C \leq 10^{-6}$ M, in $1 \times 1 \times 4$ cm spectrofluorimetric quartz cuvettes. The shape of registered fluorescence spectra was corrected for the spectral responsivity of the PTI detection system. The excitation anisotropy spectra of **1** were measured in the L-format configuration geometry [38] with corresponding extraction of a weak emission from pure solvent and scattered light. The fundamental anisotropy values, r_0 , were obtained in poly-THF (pTHF) viscous at room temperature. In this solvent, the rotational correlation time of **1**, $\theta \gg \tau$ (τ is the corresponding fluorescence lifetime), and the observed anisotropy $r = r_0/(1 + \tau/\theta) \approx r_0$ [38]. The values of fluorescence quantum yields of **1**, Φ , were determined in low concentrated solutions by a standard method relative to 9,10-diphenylanthracene in cyclohexane as a reference compound ($\Phi \approx 0.95$) [38]. Fluorescence lifetime measurements for **1** were performed with a time-correlated single photon counting system PicoHarp 300 under 76-MHz femtosecond

laser excitation (MIRA 900, Coherent) with the time resolution ≈ 100 ps. The excitation laser beam was linearly polarized and oriented by the magic angle to avoid possible artifacts in the fluorescence kinetics.

2.3. Two-photon spectral measurements

The degenerate 2PA spectrum of new probe **1** was obtained in a broad spectral range (570–970 nm) by the open-aperture Z-scan method [35] with a femtosecond laser system (Coherent, Inc.), schematically shown in Fig. 2. The output of a Ti:Sapphire laser (Mira 900-F, tuned to 800 nm, with a repetition rate $f = 76$ MHz, pulse duration $\tau_P \approx 200$ fs, and average power ≈ 1.1 W), pumped by the second harmonic of a CW Nd³⁺:YAG laser (Verdi-10), was regeneratively amplified with a 1-kHz repetition rate (Legend Elite) providing ≈ 100 fs pulses (FWHM) with the energy ≈ 3 mJ/pulse. This output at 800 nm pumped an ultrafast optical parametric amplifier (OPerA Solo) with the tuning range 0.24–20 μm , $\tau_P \approx 100$ fs (FWHM), and pulse energies, E_P , up to ≈ 100 μJ . A concentrated solution of **1** ($C \sim 10^{-2}$ M) was placed in a quartz cuvette with the path length $L = 1$ mm and moved in the caustic of a focusing Gaussian beam. Laser beam from an OPerA Solo with pulse energies $E_P \leq 100$ nJ was focused to the waist of radius $\omega_0 \sim 15$ –20 μm (depending on excitation wavelength, λ_{exc}), and condition $Z_R > L/2$ was fulfilled ($Z_R = \pi\omega_0^2/\lambda_{\text{exc}}$ – is the Rayleigh range). A compre-

hensive description of this methodology was reported previously [39–41].

2.4. Quantum chemical calculations

The electronic parameters of **1** were analyzed by quantum chemical calculations using Gaussian 2009, (Rev. A2) suite of programs [36]. The aliphatic side chains in the calculated structure were replaced with methyl groups for simplicity. The ground-state geometry was optimized at the DFT/6-31(d,p)/B3LYP level. The ZINDO method was employed to obtain the oscillator strengths, molecular orbitals, and the permanent and transition dipole moments for the optimized model structure **1**. The efficiency of 2PA processes in **1** were theoretically estimated based on the sum-over-state (SOS) approach and the simplified three-level electronic model [42, 43].

3. Results and Discussion

3.1. Linear photophysical properties of **1**

New fluorescent derivative **1** is a symmetric fluorene-based molecule containing two fluorene cores with diphenylamino end substituents connected by the central bis-diketone pyridine. The steady-state absorption and the fluorescence spectra of **1** in solvents of various polarities, Δf , are shown in Fig. 3, and its main linear photophysical parameters are presented in Table 1. As follows from Fig. 3, all absorption spectra of **1** did not reveal a vibrational structure and were nearly independent of solvent properties, except for HEX solution, where a small hypsochromic shift of ≈ 15 nm was observed. No aggregation effects in the absorption spectra were detected for the concentration range $C \leq 10^{-2}$ M. The steady-state fluorescence spectra of **1** revealed a strong solvatochromic behavior and a well-defined vibronic structure in non-polar HEX. The value of Stokes shift increased with the solvent polarity Δf up to ~ 7700 cm^{-1} , and no strict correspondence to the Lippert equation [38] was observed. The steady-state excitation spectra of **1** (Fig. 4, curves 1–4) were nearly overlapped with the corresponding absorption ones, when the observed wavelength, λ_{obs} , was set close to the fluorescence emission maximum, $\lambda_{\text{fl}}^{\text{max}}$. The excitation anisotropy spectrum in viscous pTHF (Fig. 4, curve 5) revealed a complicated nature of the main absorption band of **1**. The changes in the excitation anisotropy values, $r(\lambda_{\text{exc}})$, in the spectral range $\lambda_{\text{exc}} > 400$ nm

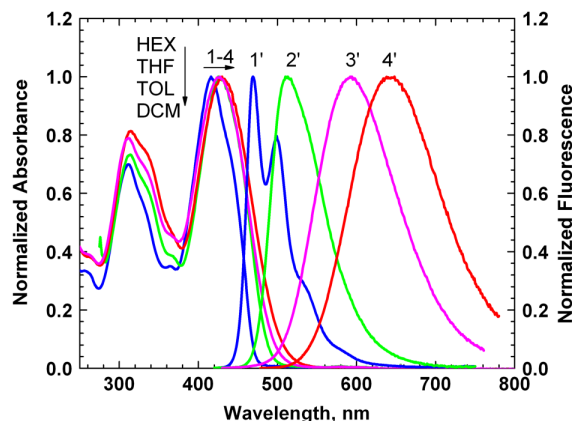


Fig. 3. Normalized linear absorption (1–4) and steady-state fluorescence (1′–4′) spectra of **1** in HEX (1, 1′), TOL (3, 3′), THF (2, 2′) and DCM (4, 4′)

are indicative of at least two electronic transitions in the main absorption band of **1**. All these data are consistent with the molecular electronic properties which can be expected for a double-chromophore structure with a weak interaction between two chromophore subsystems [44]. The values of fluorescence

Table 1. Linear photophysical parameters of **1** in organic solvents with different polarities Δf and viscosities η : absorption $\lambda_{\text{abs}}^{\text{max}}$ and fluorescence $\lambda_{\text{fl}}^{\text{max}}$ maxima, Stokes shifts, maximum extinction coefficients ϵ^{max} , fluorescence quantum yields Φ , experimental τ and calculated τ_{cal} lifetimes

N/N	HEX	TOL	THF	DCM
Δf^*	$\sim 10^{-4}$	0.0135	0.209	0.217
η , cP	0.31	0.59	0.48	0.4
$\lambda_{\text{abs}}^{\text{max}}$, nm	416 ± 1	428 ± 1	427 ± 1	430 ± 1
$\lambda_{\text{fl}}^{\text{max}}$, nm	469 ± 1	512 ± 1	592 ± 1	643 ± 1
Stokes shift, nm (cm^{-1})	53 ± 2	84 ± 2	165 ± 2	213 ± 3
$\epsilon^{\text{max}} \times 10^{-3}$, $\text{M}^{-1}\text{cm}^{-1}$	73.8 ± 5	66 ± 5	60 ± 5	60 ± 5
Φ	0.63 ± 0.06	0.66 ± 0.06	0.38 ± 0.04	0.1 ± 0.02
τ^{**} , ns	2.2 ± 0.1	2.7 ± 0.1	2.8 ± 0.1	0.97 ± 0.1
τ_{cal}^{***} , ns	1.2 ± 0.2	1.3 ± 0.2	1.3 ± 0.2	0.4 ± 0.2

*orientation polarizability $\Delta f = (\epsilon - 1)/(2\epsilon + 1) - (n^2 - 1)/(2n^2 + 1)$ (ϵ and n are the dielectric constant and the refractive index, respectively) [38].

**All experimental lifetime data correspond to goodness-of-fit parameters $\chi^2 \geq 0.98$.

*** $\tau_{\text{cal}} = \tau_R \Phi$ (where τ_R is the natural lifetime calculated by the Birks–Dyson equation [45]).

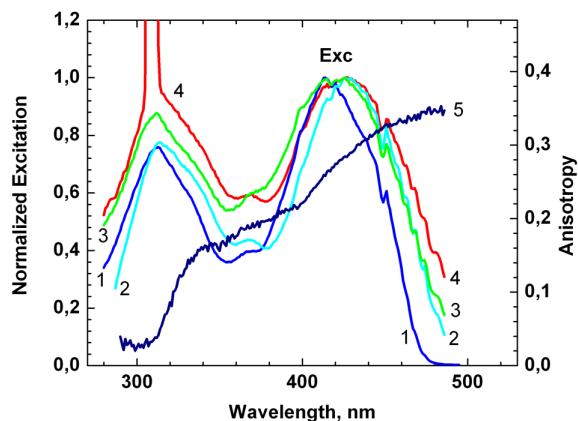


Fig. 4. Excitation spectra (1–4) and excitation anisotropy spectrum (5) of **1** in HEX (1), TOL (2), THF (3), DCM (4), and pTHF (5). Sharp peak in curve (4) corresponds to the scattering excitation line

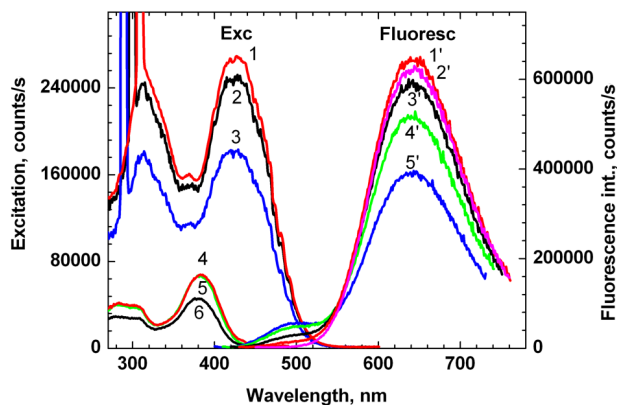


Fig. 5. Excitation (1–6) and fluorescence (1'–5') spectra of **1** in DCM with corresponding observed wavelengths $\lambda_{\text{obs}} = 620$ nm (1), 600 nm (2), 580 nm (3), 500 nm (4), 480 nm (5), 460 nm (6) and excitation wavelengths $\lambda_{\text{exc}} = 420$ nm (1'), 440 nm (2'), 410 nm (3'), 400 nm (4'), and 390 nm (5')

quantum yields of **1** are sufficiently high, $\Phi \approx 0.6$ –0.7 in HEX and TOL, and dramatically decrease with an increase of the solvent polarity in DCM. It is interesting to note that the additional fluorescence band with relatively low intensity was observed in polar DCM in a short wavelength region at $\lambda_{\text{fl}}^{\text{max}} \approx 490$ nm (Fig. 5, curves 1'–5').

The corresponding excitation spectra of this emission with the maximum at ≈ 390 nm are also shown in Fig. 5 (curves 4–6). With regard for a high cleanliness of the new synthesized material (which was confirmed by ^1H NMR, ^{13}C NMR, and high

resolution mass spectrometry), it is difficult to assume the presence of highly fluorescent impurities in this spectral range. The observed short wavelength fluorescence assumingly can be attributed to a small amount (~ 3 –5%) of highly fluorescent spatial isomers, which are characterized by a restricted π -conjugation within the central electron-donating part due to a strong solvation in polar DCM. These spatial isomers are characterized by a blue shift in the positions of their absorption peaks. Note that the excitation spectra of the short wavelength fluorescence (Fig. 5, curves 4–6) are very similar to the absorption bands of the nonsymmetric fluorene derivatives with diphenylamino end substituents [46–48], representing one chromophore of compound **1**, which is consistent with the proposed hypothesis. Another possible explanation is based on the observation of a weak fluorescence from the higher excited electronic state ($S_n \rightarrow S_0$), i.e. on the violation of Kasha's rule [38]. This hypothesis seems to be less probable due to a complicated nature of all electronic transitions of **1** involving combination of several pairs of molecular orbitals (MO) for each transition (Table 2) and a relatively high degree of the electron delocalization within MO (for more details, see results in Section 3.3). It should be mentioned that a weak short wavelength emission in nonpolar solvents is overlapped with the intensive main fluorescence band $S_1 \rightarrow S_0$ and cannot be revealed by excitation methodology.

The emission $S_1 \rightarrow S_0$ processes exhibited a single-exponential decay in all investigated solvents (Fig. 6) with corresponding lifetimes in the range $\tau \sim 0.95$ –2.8 ns (Table 1). The calculated τ_{cal} and experimental τ values of lifetimes differ by a factor of ≈ 2 due to a complicated nature of the main absorption band of **1**, including at least two electronic transitions.

3.2. 2PA efficiency of **1**

The degenerate 2PA spectrum of the new symmetric fluorene derivative **1** was obtained in a broad spectral range by the open-aperture Z-scan method and is presented in Fig. 7. As follows from these data, the 2PA spectrum of **1** revealed two well-defined absorption peaks at ≈ 320 nm and ≈ 420 nm with the maxima cross sections of $\delta_{2\text{PA}} \approx 200$ GM. The spectral position of the long wavelength 2PA contour is nearly overlapped with the main 1PA absorption band of **1**. This spectral behavior is not typical of symmet-

ric fluorene derivatives, which exhibited, as a rule, no 2PA maxima at the excitation into the main linear absorption band [48]. Assumingly, the nature of the long wavelength 2PA maximum is determined by large changes in the permanent dipole moment of **1**, $\Delta\mu_{01}$, upon the electronic excitation $S_0 \rightarrow S_1$, which are consistent with its strong solvatochromic behavior of fluorescence bands (Fig. 3). The 2PA efficiency of **1** can be analyzed by the well-known expression for a simplified three-level electronic model based on the SOS approach [42], two final states (S_1 , S_f), and one intermediate state (S_1) approximations [43, 49]:

$$\delta_{2PA} = \frac{32\pi^3}{15c^2h n^2} \times \left[\frac{E_P^2 |\mu_{01}|^2 |\mu_{1f}|^2 \Gamma_{0f} (1 + 2 \cos^2 \alpha_1)}{((E_{01} - E_P)^2 + \Gamma_{01}^2)((E_{0f} - 2E_P)^2 + \Gamma_{0f}^2)} + \frac{|\Delta\mu_{01}|^2 |\mu_{01}|^2 \Gamma_{01} (1 + 2 \cos^2 \alpha_2)}{(E_{01} - 2E_P)^2 + \Gamma_{01}^2} \right], \quad (1)$$

Table 2. Calculated positions of 1PA peaks, λ , oscillator strengths of $\pi \rightarrow \pi^*$ electronic transitions, f_{OS} , values of μ_{0i} , $\Delta\mu_{0i}$ ($i = 1-4$) and main configurations, involved into transitions, for the model compound **1** (ZINDO, Geom.[6-31(d, p)/B3LYP])

Transition	λ , nm	f_{OS}	μ_{0i} , D	$ \Delta\mu_{0i} $, D	Main configuration
$S_0 \rightarrow S_1$	402	2.50	14.6	5.0	0.40 HOMO-3→LUMO) -0.44 HOMO-2→LUMO+1)
$S_0 \rightarrow S_2$	384	0.17	3.7	5.1	0.42 HOMO-1→LUMO) -0.47 HOMO→LUMO+1) 0.38 HOMO-3→LUMO+1) 0.30 HOMO-2→LUMO)
$S_0 \rightarrow S_3$	332	0.03	1.4	1.9	-0.45 HOMO-1→LUMO+1) -0.45 HOMO→LUMO) 0.29 HOMO-2→LUMO+1) -0.40 HOMO-1→LUMO+3)
$S_0 \rightarrow S_4$	331	0.24	4.1	2.2	-0.38 HOMO→LUMO+2) 0.32 HOMO→LUMO+4) 0.31 HOMO-2→LUMO) -0.34 HOMO-1→LUMO+2) 0.30 HOMO-1→LUMO+4) -0.40 HOMO→LUMO+3)

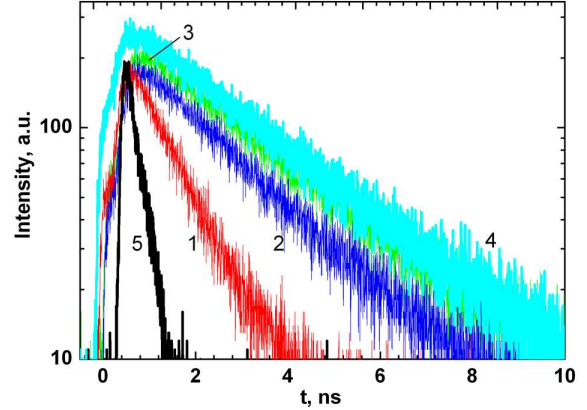


Fig. 6. Fluorescence decay curves of **1** in DCM (1), HEX (2), TOL (3), and THF (4) and the instrument response function (5)

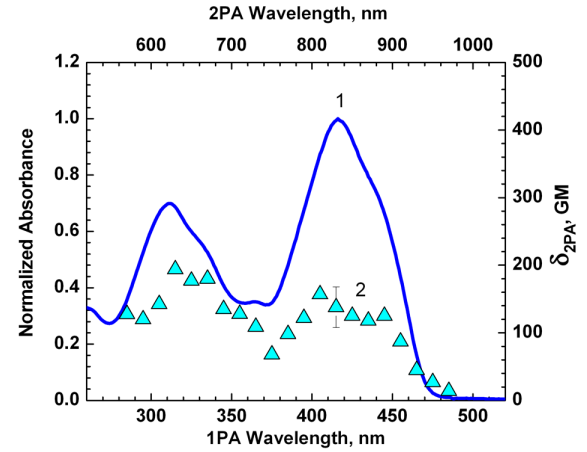


Fig. 7. 1PA (1) and 2PA (2) spectra of **1** in HEX

where c , h , and n are the velocity of light in vacuum, Planck's constant, and refractive index, respectively; $E_P = hc/\lambda_{exc}$; $E_{01} = hc/\lambda_{abs}^{max}$; μ_{01} and μ_{1f} are the transition dipoles of $S_0 \rightarrow S_1$, and $S_1 \rightarrow S_f$ electronic transitions, respectively; $\Delta\mu_{01} = \mu_0 - \mu_1$, μ_0 and μ_1 are the permanent dipole moments of S_0 and S_1 electronic states, respectively; Γ_{01} and Γ_{0f} are the damping factors for the corresponding electronic transitions; α_1 and α_2 are the angles between dipoles μ_{01} , μ_{1f} and $\Delta\mu_{01}$, μ_{01} , respectively. As follows from Eq. (1), the value of 2PA cross section under two-photon excitation in S_1 state is mainly determined by the product $|\Delta\mu_{01}|^2 \cdot |\mu_{01}|^2$ and can exhibit a separate maximum in the main linear absorption band due to a large change in the permanent dipole moment. With regard to the relatively high fluores-

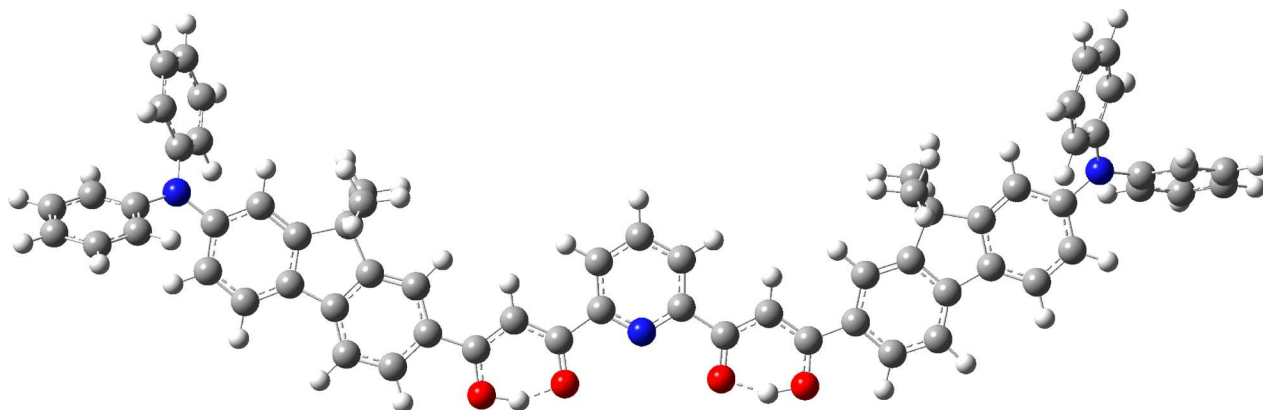


Fig. 8. Optimized molecular geometry of the model compound **1** (calculated by DFT/6-31(d,p)/B3LYP method)

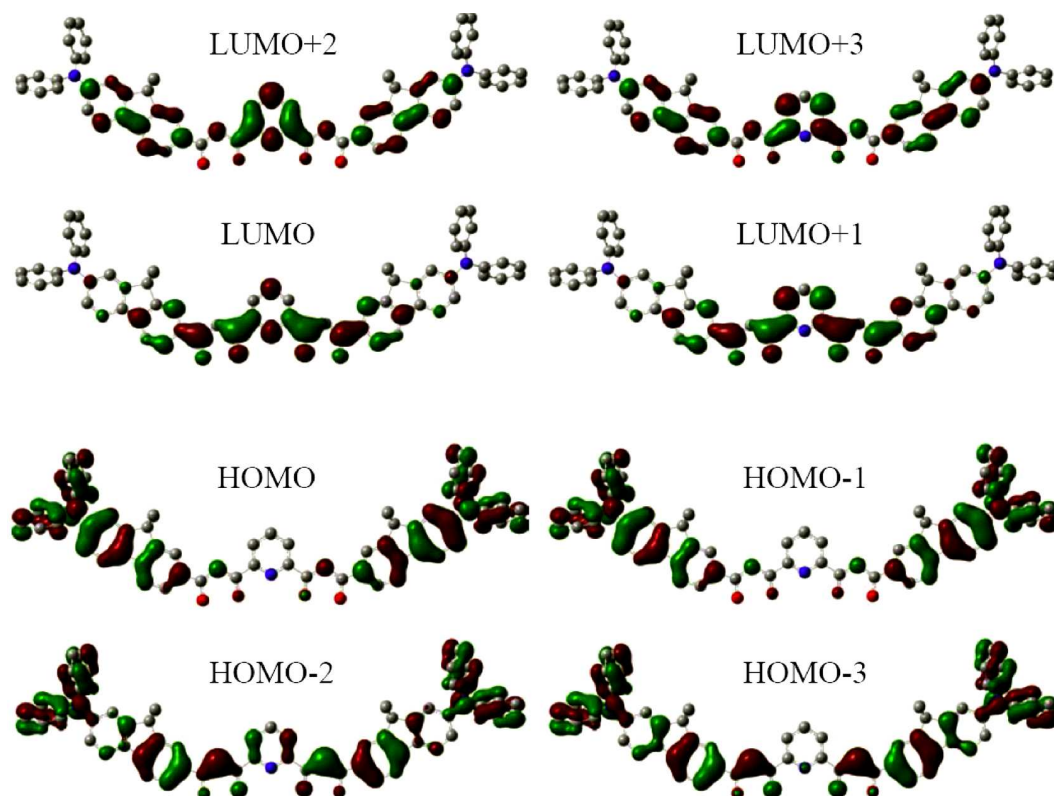


Fig. 9. Shapes of the main molecular orbitals of the model structure **1**

cence quantum yield of **1** (see Table 1), the values of two-photon action cross sections, $\delta_{2PA}^{act} = \delta_{2PA} \Phi$, were determined as $\sim 100\text{--}130$ GM, which are comparable with the corresponding values of known two-photon labels utilized in the fluorescence bioimaging technology [50, 51]. Thus, our results show that the new fluo-

rene derivative **1** has a good potential for two-photon induced fluorescence microscopy applications.

3.3. Quantum chemical analysis

The ground-state optimized geometry of **1** was obtained by the DFT/6-31(d,p)/B3LYP method and is

presented in Fig. 8. As follows from these calculations, the main chromophore is planar, and four phenyl end substituents at the nitrogen atoms are turned out at 44° relative to the chromophore plane. It should be mentioned that the planarity of the central molecular part is additionally stabilized by two hydrogen bonds between hydrogen and nearest oxygen atoms. The calculated transition wavelengths, oscillator strengths, main configurations, and other electronic parameters for the first four transitions $S_0 \rightarrow S_n$ ($n = 1-4$) of the model structure of **1** are presented in Table 2. The shapes of molecular orbitals (MO) participating in the first four electronic transitions are shown in Fig. 9. As follows from these data, the main long wavelength transition $S_0 \rightarrow S_1$ reveals a complex nature, which is based on a combination of four pairs of MO with nearly equal weight coefficients. All electronic transitions, presented in Table 2, are of the $\pi \rightarrow \pi^*$ type with noticeable oscillator strengths, especially for $S_0 \rightarrow S_1$, where $f_{OS} \approx 2.5$. It is interesting to mention that two low-energy $n \rightarrow \pi^*$ transitions with $f_{OS} \approx 0$ are also obtained from the quantum chemical calculations for the model structure **1**. These extremely weak transitions, involving the n -orbitals of oxygen atoms, assumingly can not affect the 1PA shape and the 2PA efficiency. The calculated values of 2PA cross sections, δ_{2PA} , within the main 1PA band were estimated by Eq. (1) with corresponding parameters taken from Table 1. The values obtained are in the range of $\delta_{2PA} \approx 80-160$ GM and exhibit a good agreement with the experimental 2PA data.

4. Conclusions

The synthesis and comprehensive linear photophysical and nonlinear optical studies of the new symmetric fluorene derivative **1** were performed with the goal to investigate its potential for bioimaging applications. The 1PA spectra of **1** are nearly independent of solvent properties, while the fluorescence spectra exhibit the strong solvatochromic behavior due to a large change in the permanent dipole moment at the electronic excitation $S_0 \rightarrow S_1$. The excitation anisotropy spectrum of **1** revealed a complicated nature of the main long wavelength absorption band involving at least two close-lying electronic transitions. The weak short wavelength fluorescence band was observed in a DCM solution at ≈ 500 nm

which can be attributed to a small amount of highly fluorescent isomers of **1** in polar DCM. The fluorescence lifetimes of **1** in all investigated solvents correspond to a single-exponential decay processes and exhibit a complicated dependence on the solvent polarity with a dramatic decrease of the lifetime in polar DCM. The degenerate 2PA spectrum of **1** was measured in a broad spectral range by the open aperture Z-scan method, and two well-defined 2PA bands with maximal cross sections ≈ 200 GM were obtained. The results of quantum chemical calculations revealed the nature of 1PA and 2PA transitions in a good agreement with all experimental data. Note that the long-wavelength 2PA band of **1** is overlapped with the tuning range of the commercially available Ti:Sapphire femtosecond lasers, which is important for practical purposes. The reported spectral properties along with the high fluorescence quantum yield and the 2PA efficiency strongly increase the potential of compound **1** for application in two-photon fluorescence microscopy systems, including the bioimaging technique.

We wish to acknowledge the National Academy of Sciences of Ukraine (grant 1.4.1.B/153), the National Science Foundation (ECCS-0925712, CHE-0840431, and CHE-0832622) for their support of this work.

1. Z.S. An, S.A. Odom, R.F. Kelley, C. Huang, X. Zhang, S. Barlow, L.A. Padilha, J. Fu, S. Webster, D.J. Hagan, E.W. Van Stryland, S.M.R. Wasielewski, and S.R. Marder, *J. Phys. Chem. A* **113**, 5585 (2009).
2. M. Rumi, S.J.K. Pond, T. Meyer-Friedrichsen, Q. Zhang, M. Bishop, Y. Zhang, S. Barlow, S.R. Marder, and J.W. Perry, *J. Phys. Chem. C* **112**, 8061 (2008).
3. S.A. Odom, S. Webster, L.A. Padilha, D. Peceli, H. Hu, G. Nootz, S.J. Chung, S. Ohira, J.D. Matichak, O.V. Przhonska, A.D. Kachkovski, S. Barlow, J.L. Bredas, H.L. Anderson, D.J. Hagan, E.W. Van Stryland, and S.R. Marder, *J. Am. Chem. Soc.* **131**, 7510 (2009).
4. M. Balu, L.A. Padilha, D.J. Hagan, E.W. Van Stryland, S. Yao, K. Belfield, S.J. Zheng, S. Barlow, and S. Marder, *J. Opt. Soc. Am. B* **25**, 159 (2008).
5. Q.D. Zheng, G.S. He, and P.N. Prasad, *Chem. Phys. Lett.* **475**, 250 (2009).
6. K.D. Belfield and K.J. Schafer, *Chem. Mater.* **14**, 3656 (2002).
7. C.C. Corredor, Z.L. Huang, K.D. Belfield, A.R. Morales, and M.V. Bondar, *Chem. Mater.* **19**, 5165 (2007).
8. K.J. Schafer, J.M. Hales, M. Balu, K.D. Belfield, E.W. Van Stryland, and D.J. Hagan, *J. Photoch. Photobio. A* **162**, 497 (2004).

9. K.D. Belfield, M.V. Bondar, F.E. Hernandez, and O.V. Przhonska, *J. Phys. Chem. C* **112**, 5618 (2008).
10. P.L. Wu, X.J. Feng, H.L. Tam, M.S. Wong, and K.W. Cheah, *J. Am. Chem. Soc.* **131**, 886 (2009).
11. M. Velusamy, J.-Y. Shen, J.T. Lin, Y.-C. Lin, C.-C. Hsieh, C.-H. Lai, C.-W. Lai, M.-L. Ho, Y.-C. Chen, P.-T. Chou and J.-K. Hsiao, *Adv. Funct. Mater.* **19**, 2388 (2009).
12. S.J. Andrasik, K.D. Belfield, M.V. Bondar, F.E. Hernandez, A.R. Morales, O.V. Przhonska, and S. Yao, *Chem. Phys. Chem.* **8**, 399 (2007).
13. A. Hayek, F. Bolze, J.F. Nicoud, P.L. Baldeck, and Y. Mely, *Photochem. Photobio. Sci.* **5**, 102 (2006).
14. A.R. Morales, K.J. Schafer-Hales, A.I. Marcus, and K.D. Belfield, *Bioconj. Chem.* **19**, 2559 (2008).
15. K.J. Schafer-Hales, K.D. Belfield, S. Yao, P.K. Frederiksen, J.M. Hales, and P.E. Kolattukudy, *J. Biomed. Opt.* **10**, 051402/1 (2005).
16. K. Konig, *J. Microsc.* **200**, 83 (2000).
17. R.M. Williams, W.R. Zipfel, and W.W. Webb, *Curr. Opin. Chem. Biol.* **5**, 603 (2001).
18. D.W. Piston, *Trends Cell Biol.* **9**, 66 (1999).
19. T.R. Krishna, M. Parent, M.H. Werts, L. Moreaux, S. Gmouh, S. Charpak, A.-M. Caminade, J.-P. Majoral, and M. Blanchard-Desce, *Angew. Chem. Int. Ed.* **45**, 4645 (2006).
20. C. Xu and W.W. Webb, *J. Opt. Soc. Am. B* **13**, 481(1996).
21. P. Kaatz and D.P. Shelton, *J. Opt. Soc. Am. B* **16**, 998 (1999).
22. W.J. Yang, M.S. Seo, X.Q. Wang, S.J. Jeon, and B.R. Cho, *J. Fluoresc.* **18**, 403 (2008).
23. K.D. Belfield, M.V. Bondar, O.V. Przhonska, K.J. Schafer, and W. Mourad, *J. Lumin.* **97**, 141 (2002).
24. K.D. Belfield, M.V. Bondar, O.V. Przhonska, and K.J. Schafer, *J. Fluoresc.* **12**, 449 (2002).
25. C.C. Corredor, K.D. Belfield, M.V. Bondar, O.V. Przhonska, and S. Yao, *J. Photoch. Photobio. A* **184**, 105 (2006).
26. X. Wang, S. Yao, H.-Y. Ahn, Y. Zhang, M.V. Bondar, J.A. Torres, and K.D. Belfield, *Biomed. Opt. Express* **1**, 453 (2010).
27. X. Wang, D.M. Nguyen, C.O. Yanez, L. Rodriguez, H.-Y. Ahn, M.V. Bondar, and K.D. Belfield, *J. Am. Chem. Soc.* **132**, 12237 (2010).
28. C.D. Andrade, C.O. Yanez, M.A. Qaddoura, X. Wang, C.L. Arnett, S.A. Coombs, R. Bassiouni, M.V. Bondar, and K.D. Belfield, *J. Fluoresc.* **21**, 1223 (2011).
29. K.D. Belfield, A.R. Morales, B.S. Kang, J.M. Hales, D.J. Hagan, E.W. Van Stryland, V.M. Chapela, and J. Percino, *Chem. Mater.* **16**, 4634 (2004).
30. K.D. Belfield, A.R. Morales, J.M. Hales, D.J. Hagan, E.W. Van Stryland, V.M. Chapela, and J. Percino, *Chem. Mater.* **16**, 2267 (2004).
31. J.P. Moreno and M.G. Kuzyk, *J. Chem. Phys.* **123**, 194101/1 (2005).
32. M.G. Kuzyk, *J. Chem. Phys.* **125**, 154108/1 (2006).
33. O.S. Finikova, T. Troxler, A. Senes, W.F. DeGrado, R.M. Hochstrasser, and S.A. Vinogradov, *J. Phys. Chem. A* **111**, 6977 (2007).
34. P.A. Padmawar, J.E. Rogers, G.S. He, L.Y. Chiang, L.S. Tan, T. Canteenwala, Q.D. Zheng, J.E. Slagle, D.G. McLean, P.A. Fleitz, and P.N. Prasad, *Chem. Mater.* **18**, 4065 (2006).
35. M. Sheik-Bahae, A.A. Said, T.H. Wei, D.J. Hagan, and E.W. Van Stryland, *IEEE J. Quantum Elect.* **26**, 760 (1990).
36. M.J. Frisch, G.W. Trucks, H.B. Schlegel, G.E. Scuseria, M.A. Robb, J.R. Cheeseman, G. Scalmani, V. Barone, B. Mennucci, G.A. Petersson, H. Nakatsuji, M. Caricato, X. Li, H.P. Hratchian, A.F. Izmaylov, J. Bloino, G. Zheng, J.L. Sonnenberg, M. Hada, M. Ehara, K. Toyota, R. Fukuda, J. Hasegawa, M. Ishida, T. Nakajima, Y. Honda, O. Kitao, H. Nakai, T. Vreven, J.J.A. Montgomery, J.E. Peralta, F. Ogliaro, M. Bearpark, J.J. Heyd, E. Brothers, K.N. Kudin, V.N. Staroverov, R. Kobayashi, J. Normand, K. Raghavachari, A. Rendell, J.C. Burant, S.S. Iyengar, J. Tomasi, M. Cossi, N. Rega, N.J. Millam, M. Klene, J.E. Knox, J.B. Cross, V. Bakken, C. Adamo, J. Jaramillo, R. Gomperts, R.E. Stratmann, O. Yazyev, A.J. Austin, R. Cammi, C. Pomelli, J.W. Ochterski, R.L. Martin, K. Morokuma, V.G. Zakrzewski, G.A. Voth, P. Salvador, J.J. Dannenberg, S. Dapprich, A.D. Daniels, I. Farkas, J.B. Foresman, J.V. Ortiz, J. Cioslowski, and D.J. Fox, *Gaussian* (Wallingford, CT, 2009).
37. A. Picot, C. Feuvrie, C. Barsu, F. Malvolti, B. Le Guenic, H. Le Bozec, C. Andraud, L. Toupet, and O. Maury, *Tetrahedron* **64**, 399 (2008).
38. J.R. Lakowicz, *Principles of Fluorescence Spectroscopy* (Springer, New York, 2006).
39. G. Luchita, M.V. Bondar, S. Yao, I.A. Mikhailov, C.O. Yanez, O.V. Przhonska, A.E. Masunov, and K.D. Belfield, *Appl. Mater. Interf.* **3**, 3559 (2011).
40. L.A. Padilha, S. Webster, O.V. Przhonska, H.H. Hu, D. Peceli, J.L. Rosch, M.V. Bondar, A.O. Gerasov, Y.P. Kovtun, M.P. Shandura, A.D. Kachkovski, D.J. Hagan, and E.W. Van Stryland, *J. Mater. Chem.* **19**, 7503 (2009).
41. J. Fu, L.A. Padilha, D.J. Hagan, E.W. Van Stryland, O.V. Przhonska, M.V. Bondar, Y.L. Slominsky, and A.D. Kachkovski, *J. Opt. Soc. Am. B* **24**, 67 (2007).
42. B.J. Orr and J.F. Ward, *Mol. Phys.* **20**, 513 (1971).
43. K. Ohta, L. Antonov, S. Yamada, and K. Kamada, *J. Chem. Phys.* **127**, (2007).
44. A.S. Tatikolov, Z.A. Krasnaya, L.A. Shvedova, and V.A. Kuzmin, *Int. J. Photoenergy* **2**, 23 (2000).
45. J.B. Birks and D.J. Dyson, *Proc. R. Soc. Lond. A* **275**, 135 (1963).
46. K.D. Belfield, M.V. Bondar, J.M. Hales, A.R. Morales, O.V. Przhonska, and K.J. Schafer, *J. Fluoresc.* **15**, 3 (2005).
47. K.D. Belfield, M.V. Bondar, F.E. Hernandez, A.R. Morales, O.V. Przhonska, and K.J. Schafer, *Appl. Optics* **43**, 6339 (2004).

48. K.D. Belfield, M.V. Bondar, F.E. Hernandezt, O.V. Przhonska, and S. Yao, *J. Phys. Chem. B* **111**, 12723 (2007).
49. K. Kamada, K. Ohta, Y. Iwase, and K. Kondo, *Chem. Phys. Lett.* **372**, 386 (2003).
50. O.K. Nag, C.S. Lim, B.L. Nguyen, B. Kim, J. Jang, J.H. Han, B.R. Cho, and H.Y. Woo, *J. Mater. Chem.* **22**, 1977 (2012).
51. V.L. Anderson and W.W. Webb, *BMC Biotechnol.* **11:125**, 1 (2011).

Received 23.07.12

*М.В. Бондар, О.В. Пржонська, О.Д. Качковський,
А. Фрейзер, А.Р. Моралес, К.Д. Белфілд*

НОВИЙ ФЛУОРЕСЦЕНТНИЙ ЗОНД
НА ОСНОВІ ФЛУОРЕНУ З ЕФЕКТИВНИМ
ДВОФОТОННИМ ПОГЛИНАННЯМ

Резюме

В роботі описано синтез та досліджено лінійні і нелінійно-оптичні властивості нової флуоренової молекули

3,3'-(піридин-2,6-дііл)біс(1-(7-(дифеніламіно)-9,9-дигексил-9Н-флуорен-2-іл)пропан-1,3-діон) (**1**). Було отримано та проаналізовано стаціонарні спектри поглинання, флуоресценції та анізотропії збудження нового флуорену **1** в органічних розчинниках із різною полярністю при кімнатній температурі у зв'язку з можливістю його потенційного застосування у технологіях флуоресцентної візуалізації біологічних зображень. Аналіз лінійних фотофізичних властивостей **1** розкрив складну природу основної довгохвильової смуги поглинання та показав наявність сильного сольватохромного ефекту у стаціонарних спектрах флуоресценції. Вироджені спектри двофотонного поглинання (ДФП) нового флуорену **1** були отримані у широкому спектральному інтервалі (570–970 нм) методом “Z-scan” з відкритою апертурою при 1 кГц фемтосекундному збудженні та отримано ефективні перерізи ДФП у межах 100–130 ГМ. Природа смуг лінійного поглинання молекули **1** та особливості її ДФП процесів були проаналізовані на основі квантово-хімічних розрахунків методами програмного пакета “Gaussian-09”.